Flux Saturation Length of Sediment Transport

Thomas Pähtz,[1,2,*] Jasper F. Kok,[3] Eric J. R. Parteli,[4] and Hans J. Herrmann[5,6]

[1]Department of Ocean Science and Engineering, Zhejiang University, 310058 Hangzhou, China
[2]State Key Laboratory of Satellite Ocean Environment Dynamics, Second Institute of Oceanography, 310012 Hangzhou, China
[3]Department of Atmospheric and Oceanic Sciences, University of California, Los Angeles, California 90095, USA
[4]Institute for Multiscale Simulation, Universität Erlangen-Nürnberg, Nägelsbachstraße 49b, 91052 Erlangen, Germany
[5]Departamento de Física, Universidade Federal do Ceará, 60451-970 Fortaleza, Ceará, Brazil
[6]Computational Physics, IfB, ETH Zürich, Schafmattstraße 6, 8093 Zürich, Switzerland

(Received 14 December 2012; published 20 November 2013)

Sediment transport along the surface drives geophysical phenomena as diverse as wind erosion and dune formation. The main length scale controlling the dynamics of sediment erosion and deposition is the saturation length L_s, which characterizes the flux response to a change in transport conditions. Here we derive, for the first time, an expression predicting L_s as a function of the average sediment velocity under different physical environments. Our expression accounts for both the characteristics of sediment entrainment and the saturation of particle and fluid velocities, and has only two physical parameters which can be estimated directly from independent experiments. We show that our expression is consistent with measurements of L_s in both aeolian and subaqueous transport regimes over at least 5 orders of magnitude in the ratio of fluid and particle density, including on Mars.

DOI: 10.1103/PhysRevLett.111.218002 PACS numbers: 45.70.−n, 47.55.Kf, 92.40.Gc

Sediment transport along the surface drives a wide variety of geophysical phenomena, including wind erosion, dust aerosol emission, and the formation of dunes and ripples on ocean floors, river beds, and planetary surfaces [1–6]. The primary transport modes are *saltation*, which consists of particles jumping downstream close to the ground at nearly ballistic trajectories, and *creep* (grains rolling and sliding along the surface). A critical parameter in sediment transport is the distance needed for the particle flux to adapt to a change in flow conditions, which is characterized by the *saturation length*, L_s. Predicting L_s under given transport conditions remains a long-standing open problem [6–10].

Indeed, L_s partially determines the dynamics of dunes, for instance, by dictating the wavelength of the smallest ("elementary") dunes on a sediment surface [11,12] and the minimal size of crescent-shaped barchans [11,13]. Moreover, although flux saturation plays a significant role for the evolution of fluvial sediment landscapes [14], morphodynamic models used in hydraulic engineering usually treat L_s as an adjustable parameter [15]. The availability of an accurate theoretical expression predicting L_s for given transport conditions would thus be an important contribution to the planetary, geological, and engineering sciences. In this Letter, we present such a theoretical expression for L_s. In contrast to previously proposed relations for L_s, the expression presented here explicitly accounts for the relevant forces that control the relaxation of particle and fluid velocities, and also incorporates the distinct entrainment mechanisms prevailing in aeolian and subaqueous transport (defined below).

The average momentum of transported grains per unit soil area, the sediment flux Q, is defined as $Q = MV$, where M is the mass of sediment in flow per unit soil area, and V is the average particle velocity. Since the fluid loses momentum to accelerate the particles, Q is limited by a steady-state value, the saturated flux Q_s. This flux is largely set by the fluid density ρ_f and the fluid shear velocity u_* [1–4,6], which is proportional to the mean flow velocity gradient in turbulent boundary layer flow [6]. In typical situations, such as on the streamward side of dunes, the deviation of Q from Q_s is small, that is, $|1 - Q/Q_s| \ll 1$ [10,11,16]. The rate $\Gamma(Q)$ of the relaxation of Q towards Q_s in the downstream direction (x) can thus be approximately written as [7,10,16],

$$\Gamma(Q) = dQ/dx \approxeq [Q_s - Q]/L_s, \tag{1}$$

where Γ is Taylor expanded to first order around $Q = Q_s$ [$\Gamma(Q_s) = 0$], and the negative inverse Taylor coefficient gives the saturation length, L_s. Flux saturation is controlled by the downstream evolutions of M and V towards their respective steady-state values, M_s and V_s. Changes in M with x are controlled by particle entrainment from the sediment bed into the transport layer. In the aeolian regime (dilute fluid such as air), entrainment occurs predominantly through particle impacts [6], whereas in the subaqueous regime (dense fluid such as water) entrainment occurs mainly through fluid lifting [2,3]. On the other hand, the evolution of V towards V_s is mainly controlled by the acceleration of the particles due to fluid drag, and their deceleration due to grain-bed collisions [10,12]. We note that the evolution of V is affected by changes in M and vice versa. For instance, an increase of M leads to a decrease in V in the absence of horizontal forces due to conservation of horizontal momentum. For simplicity, previous studies neglected either the saturation of V [10,17] or the relaxation of M, as well as changes in V due to grain-bed collisions [7,12]. Moreover, all previous studies did not account for the relaxation of the fluid velocity (U) towards its steady-state value (U_s) within the transport layer. This relaxation is driven by changes in the transport-flow feedback resulting from the relaxations of M and V. For instance, increasing V reduces the relative velocity $V_r = U - V$ and thus the fluid drag. In turn, as V_r decreases, the amount of momentum transferred from the fluid to the transport layer also decreases, which results in an increase in U, whereas an increase in U again increases V_r.

In this Letter, we derive a theoretical expression for L_s which encodes *all* aforementioned relaxation mechanisms. Indeed, since previously proposed relations for L_s neglect some of the interactions that determine L_s [7,10–12], it is uncertain how to adapt these equations to compute L_s in extraterrestrial environments, such as Mars [5,6,13]. Our theoretical expression overcomes this problem, since it is valid for arbitrary physical environments for which turbulent fluctuations of the fluid velocity, and thus transport as suspended load [6], can be neglected. For aeolian transport under terrestrial conditions, this regime corresponds to $u_* \lesssim 4u_t$, where u_t is the threshold u_* for sustained transport [2,3,6].

We start from the momentum conservation equation for steady ($\partial/\partial t = 0$) dilute granular flows [18],

$$\partial\rho\langle v_x^2\rangle/\partial x + \partial\rho\langle v_x v_z\rangle/\partial z = \langle f_x\rangle, \qquad (2)$$

where $\langle\rangle$ denotes the ensemble average, ρ the mass density, $\mathbf{v}$ the particle velocity, and $\mathbf{f}$ the external body force per unit volume applied on a sediment particle. Here, $\mathbf{f}$ incorporates the main external forces acting on the transported particles: drag, gravity, buoyancy, and added mass. The added mass force arises because the speed of the fluid layer immediately surrounding the particle is closely coupled to that of the particle, thereby enhancing the particle's inertia by a factor $1 + 0.5s^{-1}$, where $s = \rho_p/\rho_f$ is the grain-fluid density ratio [2]. Although this added mass effect is negligible in aeolian transport ($0.5s^{-1} \ll 1$), it affects the motion of particles in the subaqueous regime [2]. Integration of Eq. (2) over the entire transport layer depth ($\int_0^\infty ..dz$) yields,

$$\frac{d(c_v M V^2)}{dx} = \int_0^\infty \langle f_x\rangle dz + (\rho\langle v_x v_z\rangle)(0), \qquad (3)$$

where $M = \int_0^\infty \rho dz$, $V = \int_0^\infty \rho\langle v_x\rangle dz/M$, and $c_v = \int_0^\infty \rho\langle v_x^2\rangle dz/(MV^2)$. In Eq. (3), the quantity $(\rho\langle v_x v_z\rangle)(0)$ gives the difference between the average horizontal momentum of particles impacting onto $[-(\rho_\downarrow\langle v_x v_z\rangle_\downarrow)(0)]$ and leaving $[(\rho_\uparrow\langle v_x v_z\rangle_\uparrow)(0)]$ the sediment bed per unit time and soil area. This momentum change is consequence of the collisions between particles within the sediment bed ($z \leq 0$). Thus, $(\rho\langle v_x v_z\rangle)(0)$ is an effective frictional force which the soil applies on the transport layer per unit soil area. It is proportional to the normal component of the force which the transport layer exerts onto the sediment bed [3,10,19], $(\rho\langle v_x v_z\rangle)(0) = -\mu g M(s-1)/(s+0.5)$, where μ is the associated Coulomb friction coefficient, and g the gravitational constant. In order to obtain the momentum conservation equation of the particles within the transport layer from Eq. (3), we first note that $\int_0^\infty\langle f_x^{\mathrm{drag}}\rangle dz \approx (3M/4sd)C_d(V_r)V_r^2$ [19], where d is the mean grain diameter, while $C_d(V_r)$ is the drag coefficient associated with the fluid drag on transported particles, which is intermediate to fully viscous drag ($C_d \propto \nu/[V_r d]$, with ν standing for the kinematic viscosity) and fully turbulent drag (constant C_d). By further noting that the change of c_v with x is negligible (see Supplemental Material [20]), we obtain,

$$c_v\frac{d(MV^2)}{dx} = \frac{3M}{4(s+0.5)d}C_d(V_r)V_r^2 - \frac{s-1}{s+0.5}\mu g M. \qquad (4)$$

Next, we solve Eq. (4) for dV/dx thus obtaining an equation of the form $(dV/dx) = \Omega(V)$, and we expand $\Omega(V)$ around saturation, that is, $\Omega(V) \approx \Omega(V_s) + (V - V_s)d\Omega/dV|_{V_s}$. By noting that $\Gamma(V) = (dQ/dx)(V) = (M(V) + V(dM(V)/dV))\Omega(V)$ and $\Omega(V_s) = 0$, we obtain $L_s = -(d\Gamma/dQ)^{-1}|_{Q=Q_s} = -(d\Omega/dV)^{-1}|_{V=V_s}$, which leads to,

$$L_s = (s+0.5)c_v(2 + c_M)V_s V_{rs} F K[\mu(s-1)g]^{-1}, \qquad (5)$$

where $c_M = (V_s/M_s)(dM/dV)(V_s)$, and $K = \mathbf{(}1 - (dU/dV)(V_s)\mathbf{)^{-1}}$, while V_{rs} (the steady-state value of V_r) and F are given by,

$$V_{rs} = [\sqrt{8\mu(s-1)gd/9 + (8\nu/d)^2} - 8\nu/d], \quad \text{and}, \qquad (6)$$

$$F = [V_{rs} + 16\nu/d][2V_{rs} + 16\nu/d]^{-1}, \qquad (7)$$

respectively. Equations (6) and (7) result from using $C_d(V_r) = (24\nu/V_r d) + 1.5$ (valid for natural sediment [21]). We find that using other reported drag laws only marginally affects the value of L_s. Furthermore, we note that in the subaqueous regime $c_M \approx 0$, since in this regime M changes within a time scale which is more than 1 order of magnitude larger than the time scale over which Q changes [22]. This difference in time scales implies $VdM \ll dQ$ and thus $VdM \ll MdV$ in the subaqueous regime. In contrast, in the aeolian regime, $c_M \approx 1$ as the total mass of ejected grains upon grain-bed collisions is approximately proportional to the speed of impacting grains [23], which yields $M/M_s \approx V/V_s$.

In Eq. (5), the quantity K encodes the effect of the relaxation of the transport-flow feedback, neglected in previous works [7,10,17]. In the subaqueous regime, this transport-flow feedback has a negligible influence on the fluid speed [22] (and thus on its relaxation). In this regime, $(dU/dV)(V_s) \approx 0$, which yields $K \approx 1$ and thus,

$$L_s^{\text{subaq}} = [2s + 1]c_v V_s V_{rs} F[\mu(s-1)g]^{-1}. \quad (8)$$

In contrast, in the aeolian regime, U scales with the shear velocity at the bed (u_b) [19,22], and thus $(dU/dV)(V_s) \approx (U_s/u_{bs})(du_b/\mathrm{d}V)(V_s)$, where u_{bs} is the steady-state value of u_b. Using the mixing length approximation of inner turbulent boundary layer equations [24], u_b can be expressed as $u_b = u_*[1 - 3MC_d(V_r)V_r^2/(4(s+0.5)d\rho_f u_*^2)]^{1/2}$ [22]. By using this expression to compute du_b/dV and noting that $u_{bs} \approx u_t$ [6], we obtain the following expression for K,

$$K = \frac{1 + F^{-1}[(V_s + V_{rs})/(2V_{rs})][(u_*/u_t)^2 - 1]}{1 + [(V_s + V_{rs})/(2V_s)][(u_*/u_t)^2 - 1]}. \quad (9)$$

Using Eq. (9) to compute K, L_s in the aeolian regime of transport $[(s+0.5)/(s-1) \cong 1]$ is then given by

$$L_s^{\text{aeolian}} = 3c_v V_s V_{rs} FK[\mu g]^{-1}. \quad (10)$$

We show in Section IV of the Supplemental Material [20] that Eq. (10) can be approximated by the simpler form of $L_s^{\text{aeolian}} \approx 3c_v V_s^2[\mu g]^{-1}$ in the limit of large u_*/u_t.

Therefore, from our general expression for L_s [Eq. (5)] we obtain two expressions—Eqs. (8) and (10)—which can be used to predict L_s in the subaqueous and aeolian transport regimes, respectively. Both use only two parameters, namely μ and c_v, which are estimated from independent measurements. Specifically, μ is estimated from measurements of M_s and Q_s for different values of u_* in air and under water, while c_v is estimated from measurements of the particle velocity distribution [20,25,26]. From these experimental data, we obtain $\mu \approx 1.0$ (0.5) and $c_v \approx 1.3$ (1.7) for the aeolian (subaqueous) regime.

Both Eqs. (8) and (10) are consistent with the behavior of L_s with u_* observed in experiments. Indeed, L_s mainly depends on u_* via the average particle velocity, V_s. For subaqueous transport, in which V_s is a linear function of u_*, L_s varies linearly with V_s and thus with u_*, which is consistent with experiments [8]. In contrast, V_s depends only weakly on u_* for aeolian transport [6,22]. Consequently, L_s is only weakly dependent on u_* in this regime, which is also consistent with experiments [7]. In fact, when neglecting this weak dependence on u_*, Eq. (10) reduces to $L_s \propto sd$ [7,12] in the limit of large particle Reynolds numbers $\sqrt{sgd^3}/\nu$ for which $V_s \propto \sqrt{sgd}$ [22]. Moreover, we estimate the average particle velocity V_s as a function of u_*/u_t using well-established theoretical expressions which were validated against experiments of sediment transport in the aeolian or in the subaqueous regime. Specifically, we use the model of Ref. [19] for obtaining $V_s(u_*/u_t)$ in the aeolian regime and the model of Ref. [25] for the subaqueous regime [20].

The squares in Fig. 1 denote wind tunnel measurements of L_s for different values of u_*. These data were obtained by fitting Eq. (1) to the downstream evolution of the sediment flux, $Q(x)$, close to equilibrium [7]. Further estimates of L_s for aeolian transport under terrestrial conditions have been obtained from the wavelength (λ) of elementary dunes on top of large barchans [7,20]. These estimates correspond to the circles in Fig. 1, whereas the coloured lines in this figure denote $L_s/(sd)$ versus u_*/u_t predicted by Eq. (10). As we can see in Fig. 1, in spite of the scatter in the data, Eq. (10) yields reasonable agreement with the experimental data without requiring any fitting to these data. In contrast, the scaling $L_s = 2sd$ [7,12] was obtained from a fit to the data displayed in Fig. 1. Moreover, Fig. 2 shows values of L_s estimated from experiments on subaqueous transport under different shear velocities (symbols). These estimates were obtained from measurements of λ [12,27] and from the minimal cross-stream width, $W \approx 12L_s$ [13], of barchans in a water flume [8]. The colored lines show the behavior of L_s with u_* as predicted from Eq. (8) for subaqueous sand transport. We note that Eq. (8) is the first expression for L_s that shows good agreement with measurements of L_s under water. Indeed, the scaling relation $L_s = 2sd$ does not capture the increasing trend of L_s with u_*/u_t evident from the experimental data.

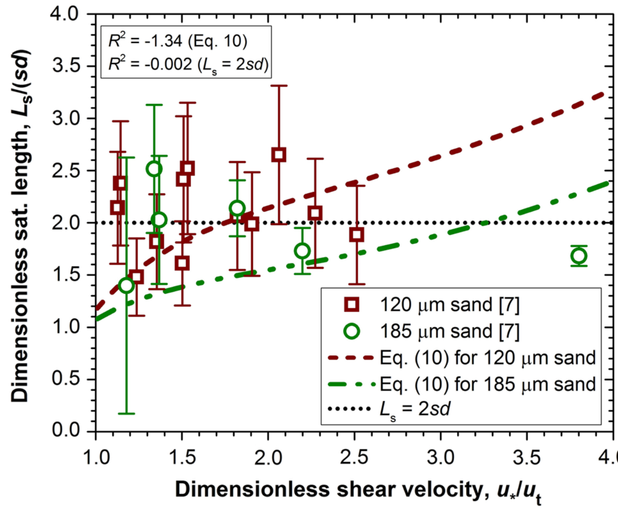

FIG. 1 (color online). Dimensionless saturation length, $L_s/(sd)$, versus u_*/u_t for aeolian transport under terrestrial conditions. Brown squares denote estimates of L_s from wind-tunnel measurements ($d = 120$ μm), while the error bars are due to uncertainties in the measurements of the sediment flux [7]. Green circles denote L_s obtained from the wavelength of elementary dunes on top of large barchans ($d = 185$ μm), whereas the error bars contain uncertainties in the dune size [7] (potential systematic uncertainties [20] are not included). The colored lines represent predicted values of L_s using Eq. (5) for the corresponding experimental conditions ($\rho_p = 2650$ kg/m^3, $\rho_f = 1.174$ kg/m^3 and $\nu = 1.59 \times 10^{-5}$ m^2/s). The dotted horizontal line indicates the prediction of L_s using $L_s = 2sd$ [7,12]. The upper legend displays the corresponding values of the coefficient of determination, $R^2 = 1 - (\sum_i (L_{si}^{\text{measured}} - L_{si}^{\text{predicted}})^2 / \sum_i (L_{si}^{\text{measured}} - L_s^{\text{mean}})^2)$, which is a measure of a theory's ability to capture variation in data, with $R^2 = 1$ corresponding to a perfect fit).

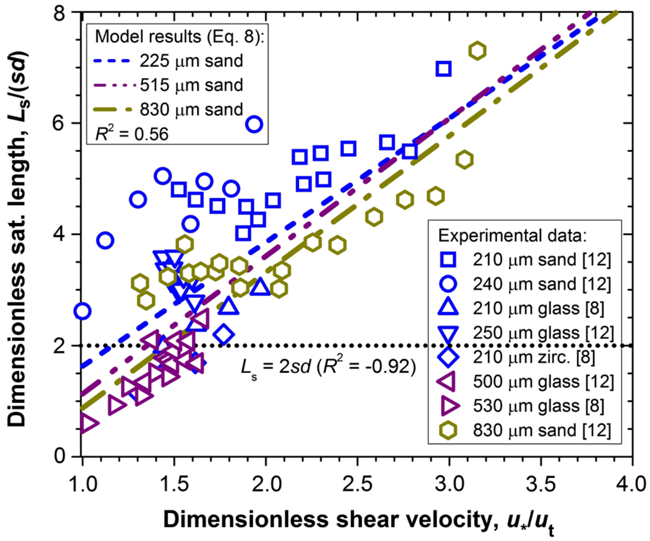

FIG. 2 (color online). $L_s/(sd)$ versus u_*/u_t for subaqueous transport. Symbols denote estimates of L_s from the wavelength of elementary dunes [12] and from the minimal cross-stream width of subaqueous barchans, $W \approx 12L_s$ [8]. The colored lines denote predicted values of L_s using Eq. (5) for subaqueous transport of sand ($\rho_p = 2650$ kg/m^3, $\rho_f = 10^3$ kg/m^3 and $\nu = 10^{-6}$ m^2/s), with grain sizes roughly matching those used in the experiments. The dotted horizontal line indicates the prediction of L_s using the scaling $L_s = 2sd$ [7,12]. The values of R^2 (coefficient of determination) for both expressions are also shown.

An excellent laboratory for further testing our model is the surface of Mars, where the ratio of grain to fluid density (s) is about 2 orders of magnitude larger than on Earth. We estimate the Martian L_s from reported values of the minimal crosswind width W of barchans at the Arkhangelsky crater in the southern highlands and at a dune field near the north pole [13,20]. However, using Eq. (10) to predict L_s on Mars is difficult because both the grain size d and the typical shear velocity $u_{*\mathrm{typ}}$ for which the dunes were formed are poorly known. Indeed, we need to know both quantities to calculate V_s [19]. We thus predict the Martian L_s using a range of plausible values of d and $u_{*\mathrm{typ}}$. Specifically, we assume d to lie in the broad range of 100–600 μm based on recent studies [5]. Estimating $u_{*\mathrm{typ}}$ on Mars is also difficult, both because of the scarcity of wind speed measurements [28], and because the threshold u_* required to initiate transport (u_{ft}) likely exceeds u_t by up to a factor of $\sim$10 [6,19,29]. We therefore calculate L_s for two separate estimates of $u_{*\mathrm{typ}}$: the first using $u_{*\mathrm{typ}} = u_{ft}$, consistent with previous studies [13,30], and the second calculating $u_{*\mathrm{typ}}$ based on the wind speed probability distribution measured at the Viking 2 landing site [20], which results in an estimate of $u_{*\mathrm{typ}}$ closer to u_t. Figure 3 shows that the values of L_s predicted with either of these estimates are consistent with those estimated from the minimal barchan width. This good agreement suggests

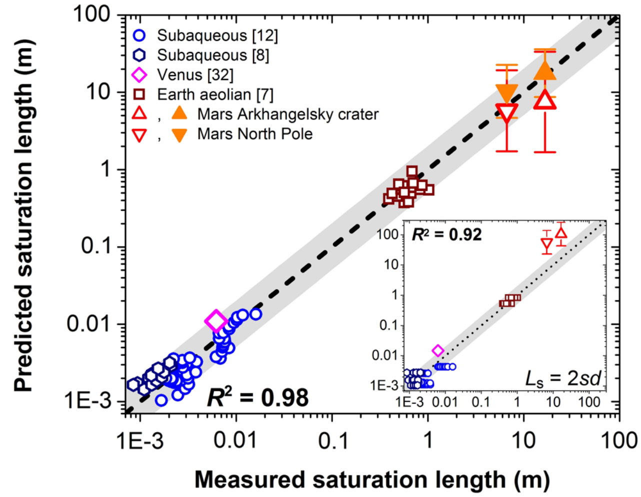

FIG. 3 (color online). Comparison of measured and predicted values of L_s for various environments; the gray shading denotes agreement between measurements and Eqs. (10) and (8) within a factor of two. Aeolian and subaqueous data were obtained as described in Figs. 1 and 2. For Venus, L_s was estimated from the wavelength of elementary dunes [20]. For Mars, L_s was derived from estimates of the minimal size of barchans in two Martian dune fields [20], and plotted against the predicted L_s for a range of plausible dune particle sizes ($d = 100$–600 μm [5]) and for two separate estimates of $u_{*\mathrm{typ}}$ (see text). The error bars denote the range in predicted L_s arising from the range in d [5], and the symbols denote the geometric mean. The filled orange symbols use $u_{*\mathrm{typ}} = u_{ft}$ [13,30], while the open red symbols use the $u_{*\mathrm{typ}}$ calculated from Viking 2 wind speed measurements [20]. The inset shows measured and predicted values of L_s for the same conditions as in the main plot, but using $L_s = 2sd$ [7,12]. Values of R^2 (coefficient of determination) in each plot were calculated in log10-space such that each data point was weighted equally.

that the previously noted overestimation of the minimal size of Martian dunes [31] is largely resolved by accounting for the low Martian value of u_t/u_{ft} [19] and the proportionally lower value of the particle speed V_s, as hypothesized in Ref. [29]. Indeed, the scaling $L_s = 2sd$ (inset of Fig. 3) requires $d \approx 29$ μm and $d \approx 40$ μm to be consistent with L_s for the north polar and Arkhangelsky dune fields, respectively. However, such particles are most likely transported as a suspended load on Mars [30], as they are on Earth [4].

Finally, Fig. 3 also compares Eq. (8) to measurements of L_s for Venusian transport, which have been estimated from the wavelength of elementary dunes produced in a wind-tunnel mimicking the Venusian atmosphere [32].

In conclusion, Eq. (5) is the first expression capable of quantitatively reproducing measurements of the saturation length L_s under different flow conditions in both air and under water, and is in agreement with measurements over at least 5 orders of magnitude of variation in the sediment to fluid density ratio. The future application of this expression thus has the potential to provide important contributions to calculate sediment transport, the response of saltation-driven wind erosion and dust aerosol emission to turbulent wind fluctuations, and the dynamics of sediment-composed landscapes under water, on Earth's surface and on other planetary bodies. The code to calculate L_s with our model is available from the first author.

We acknowledge support from Grants No. NSFC 41350110226, No. NSFC 41376095, No. ETH-10-09-2, No. NSF AGS 1137716, from the European Research Council (ERC) Advanced Grant No. 319968-FlowCCS, and DFG through the Cluster of Excellence "Engineering of Advanced Materials." We thank Miller Mendoza and Robert Sullivan for discussions, and Jeffery Hollingsworth for providing us with the pressure and temperature at the Martian dune fields.

*Corresponding author.
0012136@zju.edu.cn

[1] R. A. Bagnold, *The Physics of Blown Sand and Desert Dunes* (Methuen, London, 1941).
[2] L. C. van Rijn, *Principles of Sediment Transport in Rivers, Estuaries and Coastal Seas* (Aqua Publications, Amsterdam, 1993).
[3] M. H. Garcia, *Sedimentation Engineering: Processes, Measurements, Modeling and Practice* (ASCE, Reston, Virginia, 2007).
[4] Y. Shao, *Physics and Modelling of Wind Erosion* (Kluwer Academic, Dordrecht, 2008).
[5] M. C. Bourke, N. Lancaster, L. K. Fenton, E. J. R. Parteli, J. R. Zimbelman, and J. Radebaugh, Geomorphology **121**, 1 (2010).
[6] O. Durán, P. Claudin, and B. Andreotti, Aeolian Research **3**, 243 (2011); J. F. Kok, E. J. R. Parteli, T. I. Michaels, and D. B. Karam, Rep. Prog. Phys. **75**, 106901 (2012).
[7] B. Andreotti, P. Claudin, and O. Pouliquen, Geomorphology **123**, 343 (2010).
[8] E. M. Franklin and F. Charru, J. Fluid Mech. **675**, 199 (2011).
[9] G. S. Ma and X. J. Zheng, Eur. Phys. J. E **34**, 1 (2011).
[10] G. Sauermann, K. Kroy, and H. J. Herrmann, Phys. Rev. E **64**, 031305 (2001).
[11] K. Kroy, G. Sauermann, and H. J. Herrmann, Phys. Rev. Lett. **88**, 054301 (2002).
[12] A. Fourrière, P. Claudin, and B. Andreotti, J. Fluid Mech. **649**, 287 (2010).
[13] E. J. R. Parteli, O. Durán, and H. J. Herrmann, Phys. Rev. E **75**, 011301 (2007); E. J. R. Parteli and H. J. Herrmann, Phys. Rev. E **76**, 041307 (2007).
[14] Z. Cao, Z. Li, G. Pender, and P. Hu, Proc. ICE. Water Management **165**, 193 (2012).
[15] Z. He, W. Wu, and S. Wang, J. Hydraul. Eng. **135**, 1028 (2009); P. Hu, Z. Cao, G. Pender, and G. Tan, J. Hydrol. (Amst.) **464–465**, 41 (2012).
[16] B. M. Duc and W. Rodi, J. Hydraul. Eng. **134**, 367 (2008).
[17] F. Charru, Phys. Fluids **18**, 121508 (2006).
[18] J. T. Jenkins and M. W. Richman, Arch. Ration. Mech. Anal. **87**, 355 (1985).
[19] T. Pähtz, J. F. Kok, and H. J. Herrmann, New J. Phys. **14**, 043035 (2012).
[20] See Supplemental Material at http://link.aps.org/supplemental/10.1103/PhysRevLett.111.218002 for a description of how we estimated the model parameters c_v and μ, the average sediment velocity V_s, and the saturation length of sediment transport from the size of dunes under water and on planetary bodies.
[21] P. Y. Julien, *Erosion and Sedimentation* (Press Syndicate of the University of Cambridge, Cambridge, England, 1995).
[22] O. Durán, B. Andreotti, and P. Claudin, Phys. Fluids **24**, 103306 (2012).
[23] J. F. Kok and N. O. Renno, J. Geophys. Res. **114**, D17204 (2009).
[24] W. K. George, *Lectures in Turbulence for the 21st Century* (Chalmers University, Goethenborg, 2009), p. 125.
[25] E. Lajeunesse, L. Malverti, and F. Charru, J. Geophys. Res. **115**, F04001 (2010).
[26] M. Creyssels, P. Dupont, A. Ould El Moctar, A. Valance, I. Cantat, J. T. Jenkins, J. M. Pasini, and K. R. Rasmussen, J. Fluid Mech. **625**, 47 (2009); K. R. Rasmussen and M. Sørensen, J. Geophys. Res. **113**, F02S12 (2008).
[27] J. H. Baas, Sedimentology **46**, 123 (1999); V. Langlois and A. Valance, Eur. Phys. J. E **22**, 201 (2007).
[28] L. Sutton, C. B. Leovy, and J. E. Tillman, J. Atmos. Sci. **35**, 2346 (1978); R. Sullivan, R. Greeley, M. Kraft, G. Wilson, M. Golombek, K. Herkenhoff, J. Murphy, and P. Smith, J. Geophys. Res. **105**, 24 547 (2000); C. Holstein-Rathlou *et al.*, J. Geophys. Res. **115**, E00E18 (2010).
[29] J. F. Kok, Phys. Rev. Lett. **104**, 074502 (2010); Geophys. Res. Lett. **37**, L12202 (2010).
[30] R. E. Arvidson, E. A. Guinness, H. J. Moore, J. Tillman, and S. D. Wall, Science **222**, 463 (1983); H. J. Moore, J. Geophys. Res. **90**, 163 (1985); R. Sullivan *et al.*, Nature (London) **436**, 58 (2005).
[31] K. Kroy, S. Fischer, and B. Obermayer, J. Phys. Condens. Matter **17**, S1229 (2005).
[32] J. R. Marshall and R. Greeley, J. Geophys. Res. **97**, 1007 (1992).